Available online at www.sciencedirect.com

ScienceDirect

journal homepage: www.elsevier.com/locate/he

Ni-(Ebonex-supported Ir) composite coatings as electrocatalysts for alkaline water electrolysis. Part I: Hydrogen evolution

B.M. Jović [a], V.D. Jović [a], U.Č. Lačnjevac [a,*], Lj. Gajić-Krstajić [b], N.V. Krstajić [c]

[a] Institute for Multidisciplinary Research, University of Belgrade, Kneza Višeslava 1, 11030 Belgrade, Serbia
[b] Institute of Technical Sciences SASA, Knez Mihajlova 35, 11000 Belgrade, Serbia
[c] Faculty of Technology and Metallurgy, University of Belgrade, Karnegijeva 4, 11000 Belgrade, Serbia

ARTICLE INFO

Article history:
Received 8 April 2015
Received in revised form
23 June 2015
Accepted 24 June 2015
Available online 18 July 2015

Keywords:
Ni composite coatings
H_2 evolution
Alkaline solution
Ir catalyst
Intrinsic activity

ABSTRACT

The hydrogen evolution reaction (HER) was studied at electrodeposited Ni and Ni-(Ebonex/Ir) composite coatings in 1 mol dm^{-3} NaOH solution at 25 °C. The Ni-(Ebonex/Ir) coatings were electrodeposited from a nickel Watts type bath containing different amounts of suspended Ebonex/Ir(30 wt.%) powder particles (0–2 g dm^{-3}) onto a Ni 40 mesh substrate. The electrodes were investigated by cyclic voltammetry (CV), scanning electron microscopy (SEM), energy dispersive X-ray spectroscopy (EDS), electrochemical impedance spectroscopy (EIS) and polarization measurements. It was shown that the roughness factor of coatings increased to a maximum value of 27 with increasing the concentration of Ebonex/Ir particles in the deposition bath, while that of a pure Ni coating was found to be 3.2. In the whole potential range of the HER only one Tafel slope of about −120 mV dec^{-1} was observed at all polarization curves. Considerably improved intrinsic catalytic activity for the HER compared to pure Ni was achieved with the composite coating deposited from the bath with the lowest concentration of Ebonex/Ir particles (0.1 g dm^{-3}). Further enhancement of the apparent catalytic activity for the HER of Ni-(Ebonex/Ir) composite coatings obtained at higher concentrations of suspended Ebonex/Ir particles in the bath was attributed only to the increase of their electrochemically active surface area.

Introduction

Ni-based compounds (Ni alloys and Ni composite materials) represent the most often investigated cathode materials for the HER in alkaline solutions, mainly due to their high resistance to corrosion in concentrated alkaline solutions at elevated temperatures [1–38]. The increase of the activity of Ni-based compounds towards the HER has been achieved either by the increase of the real surface area [2,6,7,10,11,15,16,28] (in Refs. [15] and [16] porous Ni electrodes were developed and used as cathodes for the HER) or by the increase of the intrinsic activity. The intrinsic activity of Ni has been increased by depositing Ni-based composite

* Corresponding author. Tel.: +381 11 2085039; fax: +381 11 3055289.
E-mail address: uros.lacnjevac@imsi.bg.ac.rs (U.Č. Lačnjevac).
http://dx.doi.org/10.1016/j.ijhydene.2015.06.127

materials containing active solid particles [1,2,4–7,10,17–20,22–25,33,36] or by alloying Ni with other metals [8,9,11–14,21,26–30,32]. Two attempts were made to increase the catalytic activity of Ni by spontaneous deposition of Ru [34,35] or Ir [35] using a base Ni coating of high surface area as a substrate. High catalytic activity for the HER has also been obtained on the Ni-(Ebonex-supported Ru) coatings electrodeposited onto a Ni 40 mesh from the suspension containing Ebonex-supported Ru particles in the Watts type bath [36].

Iridium [39] and IrO_2 [40] electrodes, NiIr alloys [41,42] and Ir-based composite coatings [22,35,37,38] were also investigated as possible materials for hydrogen production. Boodts and Trasatti [40] studied the HER in acidic solutions at IrO_x electrodes prepared by thermal decomposition of $IrCl_3$ dissolved in water at temperatures between 300 °C and 500 °C and spread onto Ti support by a brush. It was found that thermally prepared IrO_x electrode was relatively stable in acidic solutions and that the reduction of oxide (usually unstable in acids) involved only the very surface, while the overpotential for the HER amounted to −0.1 V at 1 A cm^{-2}. Kuttiyiel et al. [37] synthesized core–shell, hollow-structured iridium–nickel nitride nanoparticles and showed that the carbon-supported deposits of these particles onto a glassy carbon electrode enhanced the HER activity in acidic solutions, being comparable to that of Pt/C catalysts. Solmaz [41] electrochemically prepared the binary NiIr coatings on a Ni-modified carbon felt substrate and investigated them as cathode materials for the HER in alkaline solutions. It was shown that a relatively low amount of electrodeposited Ir was sufficient to provide a large number of catalytically active centers at the surface of the C/Ni–NiIr electrode, thus enhancing the HER activity. Vazquez-Gomez et al. made three attempts to incorporate Ir in a rough Ni deposit [22,35,38]: Ni + IrO_2 composites [22] were electrodeposited from stirred suspensions of IrO_2 in a 0.2 M $NiCl_2$ + 2 M NH_4Cl solution, pH 4.5, at 25 °C, or in a sulfate electrolyte (0.1 M $NiSO_4$ + 1.0 M $(NH_4)_2SO_4$ + 0.7 M NH_4OH, pH 11, at 25 °C), with those obtained from chloride solution having lower overvoltage for the HER; in Refs. [35,38] porous Ni was electrodeposited at Ni rotating disc electrodes from 0.2 M $NiCl_2$ + 2 M NH_4Cl using high current densities (typically 1 A cm^{-2}) and such electrodes were either submitted to a spontaneous deposition of Ir at the open circuit potential from deaerated solutions containing 0.001 M H_2IrCl_6 at 25 °C [35], or Ir was electrodeposited from 0.002 M H_2IrCl_6 of the pH *ca.* 2.5 at 70 °C [38]. As-deposited porous Ni and Ir-modified porous Ni electrodes [35] were submitted to the same sequence of electrochemical tests in 1 M NaOH aqueous solutions (not deaerated and kept at 25 °C), with one of those tests (related to the determination of real surface area) comprising five successive cyclic voltammograms recorded between 0.2 and 0.6 V at the sweep rate of 10 mV s^{-1} to study the Ni(II)/Ni(III) reaction taking place at the electrode surface. The EIS measurements in 1 M $NaNO_3$ at the open circuit potential at 25 °C were performed to determine the electrode double layer capacity (i.e. roughness factor). It was concluded that the roughness of as-deposited Ni electrode increased with increasing time of spontaneous deposition of Ir due to Ni dissolution during the replacement reaction. Spontaneously deposited Ir did not cover the whole Ni surface and increased the total surface area (confirmed by SEM analysis). For example, after immersion of the electrode in an Ir ions containing solution for 360 min the real surface area of porous Ni increased 8.86 times according to the analysis of charge under the peaks of the Ni(II)/Ni(III) redox reaction (Q after immersion for 360 min divided by Q of as-deposited Ni, Table 1, Ref. [35]), while the EIS analysis revealed that the real surface area of porous Ni increased 46.1 times (capacity after immersion for 360 min divided by the capacity of as-deposited Ni, Table 2, Ref. [35]). Polarization curves for the HER in 1 M NaOH showed that the least negative potential of hydrogen evolution at high current densities (over −0.1 A cm^{-2}) was observed at the porous Ni + Ir coating after immersion in an Ir ions containing solution for 360 min.

In this work an attempt was made to reduce the amount of Ir for fabrication of HER cathodes by using the Ebonex particles decorated with the Ir nanoprecipitate. The Ni-(Ebonex-supported Ir) composite coatings were prepared by electrochemical codeposition of the Ni matrix and suspended Ebonex/Ir particles, and tested as catalysts for the HER in alkaline solutions.

Table 1 – Elemental composition of electrodeposited Ni-(Ebonex/Ir) samples obtained from EDS analysis.

Sample	Ni/at.%	O/at.%	Ti/at.%	Ir/at.%
2	78.6	19.6	1.55	0.20
3	88.3	9.48	1.80	0.38
4	76.5	13.0	9.70	0.83
5	72.2	15.3	11.1	1.43

Experimental

Preparation of Ebonex-supported Ir particles

Powder of Magneli phases of the general formula Ti_nO_{2n-1}, or in average Ti_4O_7 (trade name Ebonex, Altraverda, U.K.), was used in these investigations. Purchased Ebonex powder was comminuted by ball milling in isopropanol for 2 h using a Fritsch planetary mill Pulverisette 5. SEM analysis revealed that the average size of Ebonex particles reduced from 10 μm to below 5 μm after milling.

Table 2 – The values of C_{dl} and roughness factor (r_f) determined from the linear dependences $\Delta j = j_a - j_c$ vs. υ presented in Fig. 3b; Roughness factor (q_{tot}/q_{Ni}) determined from the relation of charges under the cathodic peaks for Ni(III)/Ni(II) reduction presented in Fig. 5.

Sample	C_{dl}/μF cm^{-2}	r_f	r_f/r_f(Ni)	q_c/mC cm^{-2} q vs. $\upsilon^{-1/2}$ $(\upsilon \to 0)$	
				q_{tot}	(q_{tot}/q_{Ni})
(1)	126	3.2	1	6.2	1
(2)	166	4.2	1.3	8.2	1.3
(3)	335	8.4	2.7	17.5	2.8
(4)	1073	27	8.5	57.7	9.3
(5)	1076	27	8.5	70.3	11

The iridium catalyst was deposited on the Ebonex support by a conventional impregnation method using a 2-propanol solution of Ir(III) chloride hydrate (Merck). The preparation process can be described as follows: 1.4 g of the Ebonex powder was dispersed in 100 ml of 2-propanol using an ultrasonic bath, and then mixed with the appropriate amount of $IrCl_3$ solution containing 0.6 g Ir. This suspension was ultrasonically blended for 1 h after thorough mixing. The precursor suspension was allowed to dry at 80 °C for 12 h. The precursor powder was then set in a tube furnace and reduced under flowing H_2 gas at 450 °C for 2 h and cooled to a room temperature under flowing inert (Ar) gas. The Ir loading was 30 wt.%.

Electrode preparation

The Ni-(Ebonex/Ir) samples were prepared by simultaneous electrodeposition of Ni and suspended Ebonex/Ir(30 wt.%) powder particles onto a Ni 40 mesh substrate from a conventional Watts bath of the following composition: 330 g dm^{-3} $NiSO_4 \cdot 6H_2O$ + 45 g dm^{-3} $NiCl_2 \cdot 6H_2O$ + 38 g dm^{-3} H_3BO_3. pH was kept at 4.5, while the temperature of the electrolyte was 50 °C. The amount of suspended Ebonex/Ir particles in the bath varied between 0 and 2 g dm^{-3}. Electrodeposition was carried out at a constant current density $j = -25$ mA cm^{-2} in the beaker cell of a small volume of 0.1 dm^3 with two vertical Ni mesh anodes and a Ni 40 mesh cathode between them. Thickness of the coatings was controlled through the electrodeposition charge density, which was fixed at 18.6 C cm^{-2}. Mixing of the electrolyte was provided by the air flow (1 dm^3 min^{-1}) through the spiral-shaped glass pipe with small openings facing the bottom of the cell.

The Watts type electrolyte was prepared from analytical grade chemicals dissolved in deionized water and the pH was adjusted at 4.5 by adding sodium hydroxide. Before the electrodeposition of pure Ni and Ni-(Ebonex/Ir) coatings, Ni 40 meshes were etched in 2:1 HNO_3:H_2O solution for 60 s.

For easier presentation all investigated samples are marked with the numbers: (1) – ~ 20 μm thick pure Ni deposited from the Watts bath; (2), (3), (4) and (5) – Ni-(Ebonex/Ir) samples electrodeposited from the Watts bath containing 0.1, 0.5, 1.0 and 2.0 g dm^{-3} of Ebonex/Ir(30 wt.%) powder particles, respectively.

Characterization of Ni-(Ebonex/Ir) composite coatings

The appearance of the Ebonex/Ir(30 wt.%) powder particles and Ni-(Ebonex/Ir) coatings was investigated by SEM, Tescan VEGA TS 5130 MM, while the elemental composition of samples was obtained by EDS analysis performed using a Jeol JSM 5800 SEM in conjunction with a SiLi X-Ray detector, Oxford Link Isis series 300, UK.

Electrochemical measurements and solutions

The polarization characteristics of the HER onto Ni and Ni-(Ebonex/Ir) samples were tested in 1.0 mol dm^{-3} NaOH solution in extra pure UV water (Smart2PureUV, TKA) at 25 °C. A three-compartment cell was used: the working electrode of the surface area of approximately 1 cm^2 was placed in a central compartment together with the Luggin capillary; two Pt mesh counter electrodes of larger surface areas were each placed in separate compartments (parallel to the working electrode mesh), so that the oxygen evolved at the counter electrodes could not enter the working electrode compartment. The saturated calomel electrode (SCE) was placed in a side compartment connected to the central one through a bridge and a Luggin capillary, and was kept at room temperature. All values of potential in the text are given versus the SCE. Experiments were performed using a potentiostat Reference 600 and software PHE 200 and DC 105 (Gamry Instruments). All samples were first submitted to the HER at a constant current density $j = -0.3$ A cm^{-2} for 800 s in order to reduce the Ni oxide/hydroxide present at the electrode surface to metallic Ni and to achieve a stationary value of potential (step 1), followed by conditioning at a certain constant potential for the period of 60 s sufficient to provide a stable current density response (step 2). The value of potential in step 2 was adjusted to produce cathodic current density slightly higher than −0.3 A cm^{-2}. After such pre-electrolysis, polarization curves were recorded by sweeping the potential at 1 mV s^{-1} from the value applied in step 2 to the value of open circuit potential. During the course of the sweeps, potential was automatically corrected for the *IR* drop using the current interrupt technique.

The EIS measurements were performed with the same potentiostat and EIS 300 software, applying the amplitude of 5 mV RMS in the frequency range from 10 kHz to 0.01 Hz with 20 points per decade. EIS spectra were recorded at four different potentials for each Ni-(Ebonex/Ir) sample. The potentials for presenting C_{dl} vs. *E* and *E* vs. log ($1/R_F$) dependences (Figs. 10 and 11, respectively) were corrected for the *IR* drop using the corresponding values of stationary current density and the solution resistance determined from the Nyquist plots. The real (Z′) and imaginary (Z″) components of electrochemical impedance spectra in the Nyquist plot were analyzed using the complex nonlinear least squares (CNLS) fitting program (EIS 300) to simulate the equivalent resistances and capacitances.

The CV curves used for determining the double layer capacity (i.e. roughness factor) of all investigated samples were recorded at various sweep rates (from 20 to 500 mV s^{-1}) in the potential range from −0.45 V to −0.30 V. The double layer capacity was determined from the slope of the linear dependence $\Delta j = j_a - j_c$ vs. υ [43]. CV experiments were also performed in the potential range from −1.0 V to 0.5 V at different sweep rates. Before recording the CVs, all electrodes were submitted to 30 cycles at $\upsilon = 100$ mV s^{-1} in the same potential range. In the case of electrodes with high current densities for Ni(II)/Ni(III) peaks (over 10 mA cm^{-2}), CVs were corrected for the *IR* drop by using a positive feedback technique (*R* was determined from EIS measurements and CVs were automatically corrected for the *IR* drop during cycling).

Results and discussion

SEM-EDS characterization

The microstructure of the prepared Ebonex/Ir powder can be seen in the backscattered electron (BSE) SEM image in Fig. 1. Our expectation that all Ebonex particles would be uniformly

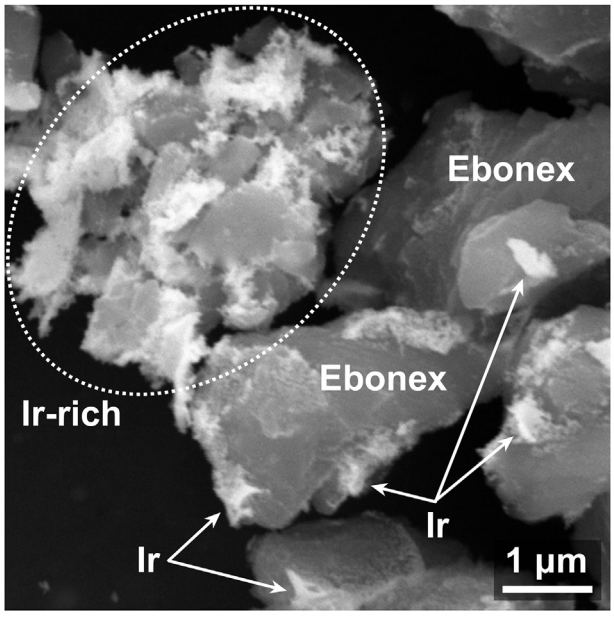

Fig. 1 – Typical example of the microstructure of Ebonex/Ir(30 wt.%) powder with marked Ebonex particles and Ir nanoparticles, while the core–shell structure is marked with an ellipse.

covered with Ir nanoparticles, forming a core–shell structure, was only partially fulfilled. As illustrated in Fig. 1, Ir nanoparticles were non-uniformly distributed on top of the Ebonex substrate. Only a fraction of the Ebonex surface was decorated with Ir agglomerates (white areas), while the rest of Ebonex particles remained uncovered (gray areas). EDS analysis of the Ebonex/Ir powder revealed that the average weight percent ratio between Ti and Ir was 61:39, which is very close to the Ti:Ir ratio of 60:40 that was calculated for the nominal Ir loading of 30 wt.% and taking Ti_4O_7 as the average chemical formula of Ebonex. Hence, the prepared powder was denoted as Ebonex/Ir(30 wt.%).

The morphology of coatings electrodeposited from a Watts bath containing different amounts of suspended Ebonex/Ir particles (0–2 g dm^{-3}) onto Ni 40 mesh is presented in Fig. 2. A typical compact Ni deposit was obtained from a blank Watts bath (Fig. 2a). The appearance of coatings significantly changed upon addition of Ebonex/Ir(30 wt.%) powder in the bath. The coating obtained at the lowest concentration of suspended Ebonex/Ir(30 wt.%) of 0.1 g dm^{-3} was characterized by the presence of two distinctive parts on the Ni 40 mesh support: the compact Ni deposit and the dispersed deposit consisting of Ebonex/Ir particles embedded in the electrodeposited Ni matrix (Fig. 2b). Higher concentrations of suspended Ebonex/Ir(30 wt.%) powder resulted in increased coverage of Ni 40 mesh with a composite Ni-(Ebonex/Ir) deposit (Fig. 2c–e). Fig. 2d and e show that the Ni 40 mesh in samples obtained from a Watts bath containing 1.0 g dm^{-3} and 2.0 g dm^{-3} of Ebonex/Ir(30 wt.%), respectively, was completely covered with a rough Ni-(Ebonex/Ir) composite deposit of high surface area. Ir particles present on the outer surface of the porous composite structures can be detected as white spots in the BSE image given in Fig. 2f.

The composition of Ni-(Ebonex/Ir) composite deposits was examined by EDS and the results (in at.%) are collected in Table 1. It is evident that Ni was the main constituent of all composite deposits (above 70 at.%). The content of Ir was found to steadily increase with the increase of the concentration of Ebonex/Ir powder particles suspended in the deposition bath, but it was generally very low (maximum 1.43 at.% Ir for sample 5). For comparison, the Ni-(Ebonex/Ru) composite coatings prepared under similar experimental conditions possessed a higher content of a noble metal catalyst, *e.g.* maximum 2.1 at.% Ru for the sample deposited from a Watts bath with 5 g dm^{-3} of Ebonex/Ru particles [36]. Based on these findings it can be inferred that the rate of incorporation of suspended particles was higher in the case of Ni-(Ebonex/Ru) composite coatings than for the electrodeposition of Ni-(Ebonex/Ir) composite coatings. Vazquez-Gomez et al. [22] also showed that the volume fraction of IrO_2 incorporated in the Ni + IrO_2 electrodeposited composites was comparably lower than that of RuO_2 in the Ni + RuO_2 composites owing to the poor incorporation rate of IrO_2 particles. Nevertheless, it appears that even such a small amount of incorporated Ebonex/Ir particles was sufficient to alter the mechanism of Ni deposition from a Watts bath, producing three-dimensional composite coatings with considerable surface roughness.

Results of CV investigations

In order to determine roughness factor for each electrode surface, CVs for all investigated samples were recorded at various sweep rates in the potential range from −0.45 V to −0.30 V. Each electrode was left in a N_2 purged solution at the open circuit potential for 1 h before recording the above mentioned CVs, with no previous treatment. One example for the sample deposited from the Watts bath containing 1.0 g dm^{-3} of Ebonex/Ir particles (sample 4) is presented in Fig. 3a. Flat CVs, typical for double layer charging/discharging, were obtained for all samples. The values of the double layer capacity (C_{dl}) were obtained from the slopes of $\Delta j = j_a - j_c$ vs. υ dependences [43] presented in Fig. 3b ($\Delta j/\Delta\upsilon = 2C_{dl}$). The values of roughness factor (r_f) were obtained by dividing measured C_{dl} values with 40 μF cm^{-2} (the value of ideally flat Ni electrode [44]) and corresponding results are given in Table 2.

Fig. 4a shows the shapes of the CVs for Ni and Ni-(Ebonex/Ir) composite coatings recorded at the sweep rate of 100 mV s^{-1}, while in Fig. 4b are shown CVs for Ni and a Ni-(Ebonex/Ir) composite coating (sample 3) recorded at the sweep rate of 40 mV s^{-1} which provided better resolution of the corresponding anodic and cathodic peaks. There is a significant increase of the voltammetric charges at Ni-(Ebonex/Ir) composite coatings electrodeposited from the bath which contained a higher concentration of suspended Ebonex/Ir particles (Fig. 4a). The improvement of voltammetric responses is a result of increasing roughness of composite coatings, as SEM analysis also suggested.

CVs recorded on Ni and Ni-(Ebonex/Ir) coatings were characterized by a different number of anodic and cathodic peaks, as seen in Fig. 4b. Peaks Ia, IIc and IIIc, common to both electrodes, refer to the highly reversible anodic and cathodic processes described by the equation:

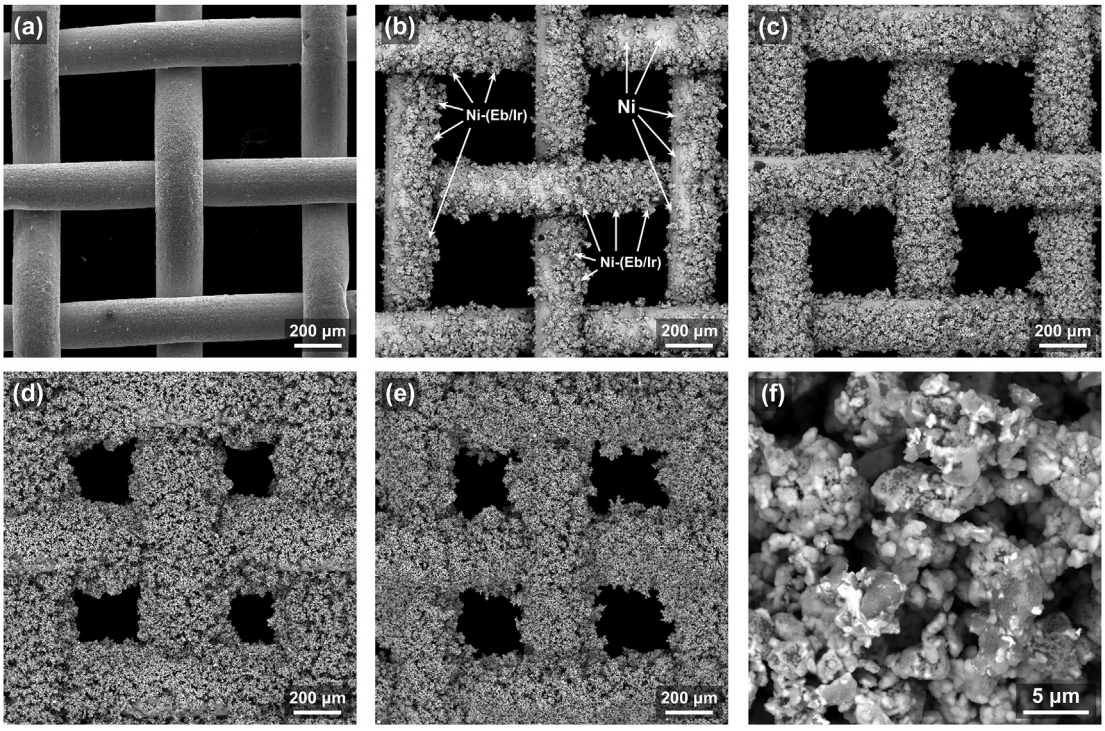

Fig. 2 – The appearance of coatings electrodeposited onto Ni 40 mesh from a nickel Watts bath containing different concentrations of suspended Ebonex/Ir particles: (a) 0 g dm^{-3} (sample 1, pure Ni); (b) 0.1 g dm^{-3} (sample 2); (c) 0.5 g dm^{-3} (sample 3); (d) 1.0 g dm^{-3} (sample 4); (e) 2.0 g dm^{-3} (sample 5). Note that compact Ni and dispersed composite Ni-(Ebonex/Ir) deposits in (b) are marked with arrows. (f) Typical morphology of the Ni-(Ebonex/Ir) composite structure at higher magnification.

$$\beta - Ni(OH)_2 + OH^- \Leftrightarrow (\beta,\gamma) - NiOOH + H_2O + e^- \quad (1)$$

where the solid state diffusion of H^+ ions is the rate determining step. Accordingly, anodic peak Ia can be attributed to the oxidation of $Ni(OH)_2$ to NiOOH, while the cathodic peaks can be identified as the reduction of β-NiOOH (peak IIc) and γ-NiOOH (peak IIIc) [45]. Thus, the charges obtained under cathodic peaks IIc and IIIc represent the amount of β-NiOOH and γ-NiOOH produced during the anodic potential sweep. Anodic peak IIa and corresponding cathodic peak Ic were observed only at Ni-(Ebonex/Ir) composite coatings and could be assigned to the surface redox reactions involving iridium oxides species.

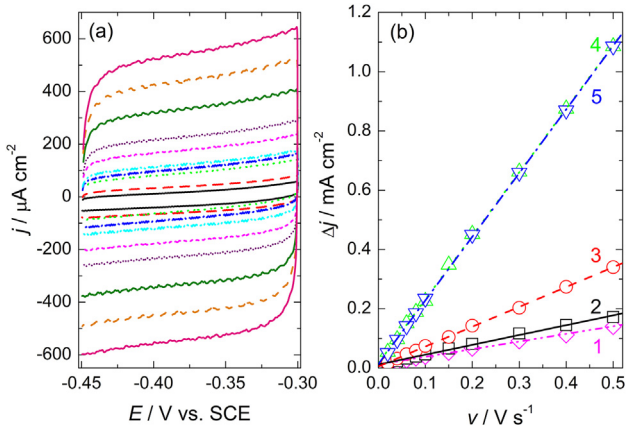

Fig. 3 – (a) CVs of sample (4) recorded in the potential range from −0.45 V to −0.30 V at different sweep rates (from 20 to 500 mV s^{-1}). (b) The $\Delta j = j_a - j_c$ vs. v dependences obtained by the analysis of CVs recorded for all investigated samples.

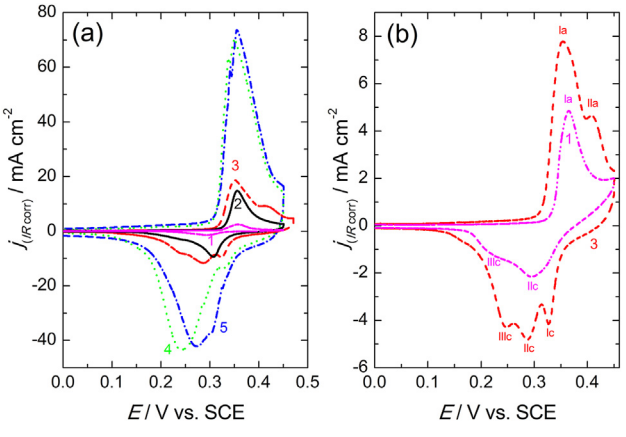

Fig. 4 – (a) CVs of Ni-(Ebonex/Ir) samples recorded in the potential range from 0.0 V to 0.5 V at the sweep rate of 100 mV s^{-1} (b) CVs of pure Ni (sample 1) and sample 3 recorded in the potential range from 0.0 V to 0.5 V at the sweep rate of 40 mV s^{-1} with corresponding anodic and cathodic peaks marked in the figure.

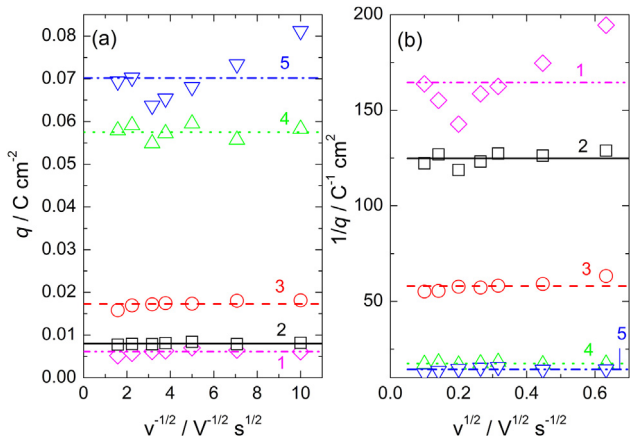

Fig. 5 – Dependences of q vs. $v^{-1/2}$ (a) and $1/q$ vs. $v^{1/2}$ (b) obtained by the analysis of charges under cathodic peaks for all samples.

The ratio between the active surface areas of the investigated electrodes can be estimated from the ratio between the corresponding cathodic charges for the reduction of NiOOH to β-$Ni(OH)_2$. The anodic and cathodic current peaks are proportional to a square root of the sweep rate (v), which is not surprising, taking into account that both reactions (Eq. (1)) are diffusion controlled. In this case it is easy to show that the cathodic charge (q) should be a linear function of $v^{-1/2}$ and the reciprocal charge ($1/q$) should be a linear function of $v^{1/2}$ [46]. Fig. 5 shows that linearity is indeed observed.

Extrapolation of the q vs. $v^{-1/2}$ line to $v^{-1/2} \rightarrow 0$ gives the fraction of the total charge which corresponds to the infinitely large sweep rate (q_s). It is assumed in this case that the charging or discharging processes are able to reach equilibrium only on the "outer" surface of the coating. At the same time, extrapolation of $1/q$ vs. $v^{1/2}$ line to $v^{1/2} \rightarrow 0$ gives the charge at the infinitely slow sweep rate (q_{tot}). In this case, the charging process is able to reach equilibrium not only on the "outer" surface area, but also inside both meso- and micropores that represent the so-called "inner" part of the total surface area. By comparing limiting values obtained for both dependences it could be concluded that the total charge (q_{tot}) is practically equal to the charge of the "outer" surface area (q_s), indicating that all Ni-(Ebonex/Ir) coatings possessed well-developed active surface areas and that the whole surface was accessible to the electrochemical reaction. As can be seen in Table 2, the ratio q_{tot}/q_{Ni} is almost identical to the ratio r_f/r_f(Ni), except for the sample (5), indicating that roughness factor could be determined by either of these two approaches.

Polarization curves for the HER

An interesting phenomenon was detected while recording polarization curves for the HER. It was observed that Ni-(Ebonex/Ir) coatings became more active for the HER after 10 successive cycles ($v = 100$ mV s^{-1}) in the potential range from −1.0 V to 0.7 V. CVs of "activation" for sample (4) are presented in Fig. 6, while polarization curves before and after "activation" are shown in the inset of Fig. 6. Hence, all samples were subjected to "activation" before recording polarization curves for the HER, i.e. all electrodes were submitted to 10 cycles with $v = 100$ mV s^{-1} in the potential range from −1.0 V to 0.7 V.

In the explored potential range extending to 0.7 V both Ni oxidation and growth of surface oxides on Ir should be expected. Thus, it can be concluded that after activation of electrodes the HER took place at the surface of reduced iridium hydroxide/oxide. It is well known that hydrous iridium oxide film is highly resistant to the reduction under cathodic hydrogen evolution conditions in aqueous acidic or basic solutions. It has been suggested [40] that the barrier to reduction is attributed to the involvement of high energy

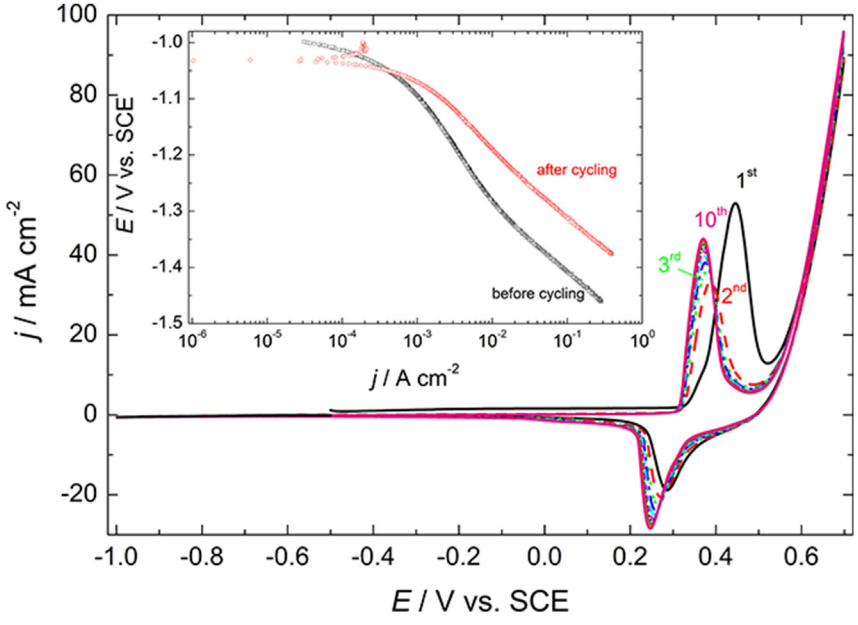

Fig. 6 – CVs of "activation" for sample 4 recorded with the sweep rate of 100 mV s^{-1}. Inset: Corresponding polarization curves for the HER.

intermediates (iridium atoms) which can only be generated at unusually negative overpotential values evidently far into the HER potential range.

The activation by oxidation of porous Ni cathodes modified by Ir has already been observed [38]. According to [40], the activation could be related to the wetting phenomena and to the surface modifications. Wetting of the inner surface of the Ni-(Ebonex/Ir) electrode is apparently promoted by a reduction and reoxidation during CV measurements, which enables the solution to spread inside the pores by changing hydrophobic into hydrophilic sites.

Polarization curves for the HER recorded for all investigated samples are shown in Fig. 7a. It is obvious that the incorporation of Ebonex-supported Ir particles in the Ni deposit caused a significant improvement in the current density for the HER, with the HER potential becoming more positive as the concentration of Ebonex/Ir particles suspended in the deposition bath increased from 0 g dm^{-3} (sample 1, pure Ni) to 2.0 g dm^{-3} (sample 5). Taking into account that roughness factor of the coatings also increased with the amount of incorporated Ebonex/Ir particles, the observed increase in rate of the HER could be primarily ascribed to the increase of active surface area. In order to elucidate the sources of apparent activity, measured current densities (j_m) were divided by the corresponding values of roughness factor (Table 1) and presented in Fig. 7b (denoted as j_m/r_f). In such a way the intrinsic catalytic activity, represented as "intrinsic current density", was obtained. As can be seen in Fig. 7b, the polarization curves of all Ni-(Ebonex/Ir) electrodes practically overlapped after correction for the surface roughness effects. It appears that the addition of only 0.1 g dm^{-3} Ebonex/Ir particles in the nickel Watts bath was enough to achieve the maximum intrinsic catalytic activity for the HER of electrodeposited composite coatings. Hence, the increase in apparent activity for the HER at the Ni-(Ebonex/Ir) electrodes can be attributed solely to the increase of their electrochemically active surface area. A large difference in intrinsic catalytic activity for the HER between pure Ni and Ni-(Ebonex/Ir) composite cathodes can also be observed in Fig. 7b. Since Ebonex, as electrode material, exhibits very low activity for electron transfer reactions [47], the enhanced intrinsic catalytic properties of Ni-(Ebonex/Ir) cathodes compared to pure Ni can be associated with the presence of iridium hydroxide/oxide at the surface.

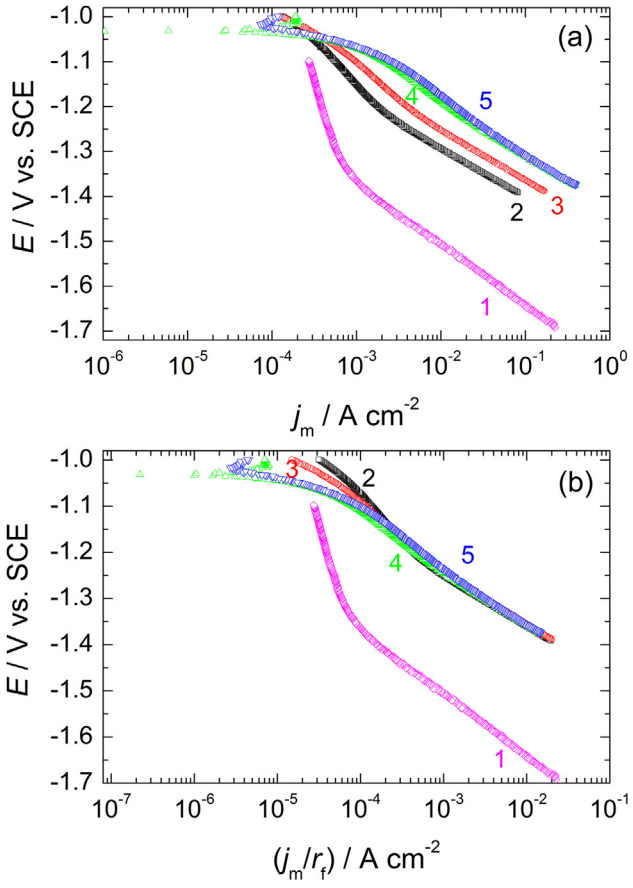

Fig. 7 – (a) Polarization curves for all investigated samples recorded at the sweep rate of 1 mV s^{-1}. (b) The same polarization curves corrected for the r_f.

In the whole potential range of the HER only one Tafel slope of about −120 mV dec^{-1} is present at the polarization curves for all investigated samples (Fig. 7a). Boodts and Trasatti [40] proposed a mechanism for the HER on metal oxide electrodes in acidic solutions, in which the first step is the electrochemical reduction of the surface active sites, M-OH. The general mechanism adopted for the alkaline solutions may be the following one:

$$M-OH + H_2O + e^- \rightarrow M-OH_2^* + OH^- \quad (2)$$

$$M-OH_2^* \rightarrow M-OH_2 \quad (3)$$

$$M-OH_2 + e^- \rightarrow M-H + OH^- \quad (4)$$

$$M-H + H_2O \rightarrow M-OH + H_2\uparrow \quad (5)$$

Step (3) accounts for possible spillover effects (surface chemical rearrangements). Step (4) involves further electrochemical reduction of the reduced Ir surface complex, Ir–OH_2, with the formation of adsorbed hydrogen. For all investigated catalysts, the first step in the mechanism (Eq. (2)), which represents the electrochemical reduction of active sites, is the rds, corresponding to the Tafel slope of −120 mV dec^{-1}.

EIS results

EIS measurements were performed on Ni-(Ebonex/Ir) electrodes at four *IR*-uncorrected potentials, −1.15 V, −1.20 V, −1.25 V and −1.30 V, covering current density range from about −1 mA cm^{-2} to about −50 mA cm^{-2}. In Fig. 8a are presented Nyquist plots recorded for sample (3) at all four selected potentials, while in Fig. 8b are presented Nyquist plots recorded at the potential $E = -1.25$ V for all Ni-(Ebonex/Ir) samples. Experimental points are presented with symbols (squares, circles, triangles, etc.), while fitted curves are presented with lines. All Nyquist plots were characterized by only one apparent arc or semicircle. The best fit at $E = -1.15$ V was obtained using the equivalent circuit presented in Fig. 9a, typical for the HER [48]. The HER kinetics-related part of this circuit consists of elements $R_p\|C_p$ in series with R_{ct}, where

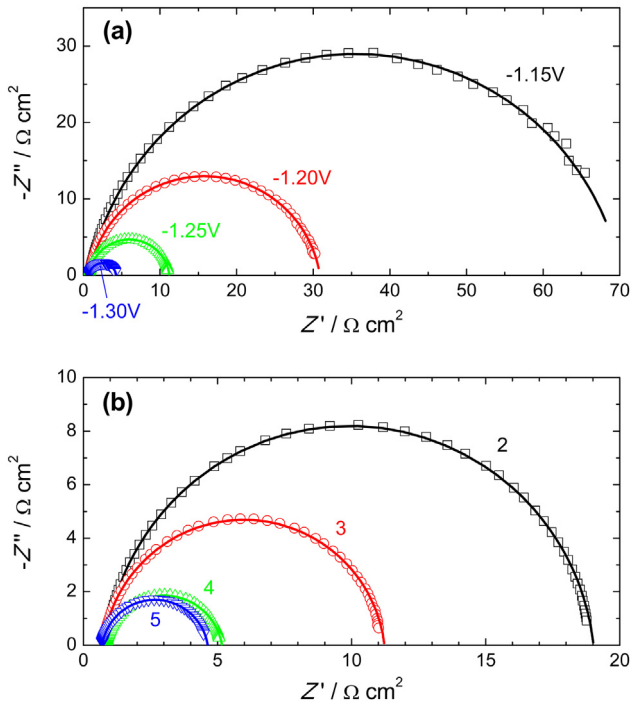

Fig. 8 – (a) Nyquist plots recorded at four different potentials (marked in the figure) for sample 3. (b) Nyquist plots recorded at the potential $E = -1.25$ V for all Ni-(Ebonex/Ir) samples (marked in the figure).

parameters R_p and C_p are associated with the relaxation of the adsorbed reaction intermediate upon potential perturbation [49], and R_{ct} is the charge transfer resistance, while CPE_{dl} is a constant phase element replacing C_{dl}, and R_s is the solution resistance. The impedance of CPE_{dl} is given as [50].

$$Z_{CPE_{dl}} = \frac{1}{Y_{dl}(j\omega)^{\alpha_{dl}}} \quad (6)$$

where Y_{dl} is a capacitance parameter (in $\Omega^{-1}\,cm^{-2}\,s^{\alpha}$) and α_{dl} is a parameter associated with a constant phase angle $\varphi = -(90\alpha_{dl})^{\circ}$, having a value between 0 and 1. At other three, more negative, potentials the contribution of parameters R_p and C_p to the total impedance response was negligible, so the model used for fitting was reduced to a simple Randles circuit

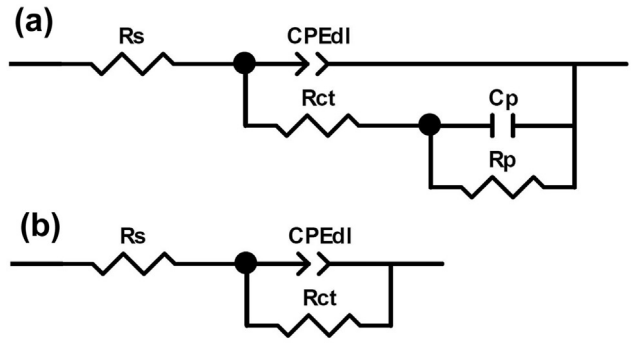

Fig. 9 – Equivalent circuits used for modeling of EIS spectra for Ni-(Ebonex/Ir) samples acquired at different potentials: (a) −1.15 V; (b) −1.20, −1.25 and −1.30 V.

(Fig. 9b). Parameters obtained from the fitting procedure are presented in Table 3.

Values of C_{dl} were calculated using the equation [51]:

$$C_{dl} = \left[Y_{dl}\left(\frac{1}{R_s} + \frac{1}{R_{ct}}\right)^{(\alpha_{dl}-1)}\right]^{1/\alpha_{dl}} \quad (7)$$

and the corresponding fitted parameters are given in Table 3. The dependence of C_{dl} on potential (*IR* corrected, see Section 2.4.) for various Ni-(Ebonex/Ir) samples is graphically presented in Fig. 10. As expected for the HER on porous electrodes, C_{dl} for each sample decreased with increasing cathodic potential due to the blocking effect of hydrogen bubbles evolved at higher current densities. However, the ratio between the C_{dl} values of investigated samples essentially did not vary with potential and was similar to the ratio between the C_{dl} values obtained from the analysis of the double layer charging/discharging or the cathodic voltammetric charges in the $NiOOH/Ni(OH)_2$ region (see Table 2). It can also be observed that the absolute C_{dl} values of Ni-(Ebonex/Ir) samples obtained from the EIS analysis were comparably higher. This finding supports the assumption that the CV activation treatment improved the hydrophilicity of the surface sites and increased the portion of the inner surface area of Ni-(Ebonex/Ir) porous structures that was in contact with aqueous alkaline solution. It should be emphasized that the non-existence of high frequency semicircles in the Nyquist plots that are related to the pore resistance is in good agreement with the results of the voltammetric charge analysis, i.e. not only the outer surface but also the inner surface of investigated Ni-(Ebonex/Ir) electrodes exhibited accessibility to different electrochemical processes.

Fig. 11 shows the relationship between the potential and the Faradaic resistance to the HER, $R_F = R_{ct} + R_p$, obtained for all Ni-(Ebonex/Ir) samples by modeling of EIS data. As can be seen, all E vs. log R_F dependences were linear and characterized by a slope of about −120 mV/dec, similarly to the Tafel plots obtained in polarization measurements (see Fig. 7). The parallelism of E vs. log R_F dependences corresponding to different samples confirm the dominant role of surface roughness effects in the apparent activity for the HER of Ni-(Ebonex/Ir) composite cathodes.

The catalytic performance of the Ni-(Ebonex/Ir) electrode with 5.2 wt% Ir (sample 5, 1.43 at.% Ir) was comparable to the C/Ni–NiIr composite electrode containing 3.9 wt% Ir [41]. For example, the HER charge transfer resistance for sample 5 at the potential of −1.30 V vs. SCE was 1.68 Ω cm^2 (Table 3), while that for C/Ni–NiIr at the potential of −1.285 V vs. SCE was calculated to be 1.8 Ω cm^2 taking into account the average weight and dimensions of the carbon felt substrates [41]. The potential of −1.31 V vs. SCE corresponding to the HER current density of −100 mA cm^{-2} in a 1 M NaOH solution was recorded both on sample 5 and the best porous Ni + IrO_2 composite cathode electrodeposited from a chloride bath and characterized by the volume fraction of incorporated IrO_2 of 0.35 [22]. Compared to the Ni-(Ebonex/Ir) electrodes, the porous Ni electrodes modified by spontaneous deposition of Ir [35] or cathodic deposition of Ir [38] exhibited superior activity for the HER, being about −1.085 V vs. SCE@-100 mA cm^{-2}. The authors, however, did not present any fraction of Ir in those

Table 3 – Parameters obtained by fitting EIS spectra with the equivalent circuits presented in Fig. 9.

Sample	E/V	$R_s/\Omega\ cm^2$	$R_p/\Omega\ cm^2$	$C_p/mF\ cm^{-2}$	$R_{ct}/\Omega\ cm^2$	$Y_{dl}/m\Omega^{-1}\ cm^{-2}\ s^{\alpha}$	α_{dl}
(2)	−1.15	0.806	8.24	12.1	124	1.07	0.876
	−1.20	0.812	–	–	55.8	0.725	0.902
	−1.25	0.833	–	–	18.2	0.472	0.934
	−1.30	0.849	–	–	5.85	0.349	0.961
(3)	−1.15	0.724	–	–	69.5	2.38	0.884
	−1.20	0.724	–	–	30.2	1.63	0.905
	−1.25	0.733	–	–	10.5	1.11	0.929
	−1.30	0.743	–	–	3.51	0.864	0.947
(4)	−1.15	0.857	15.0	0.798	5.98	4.68	0.893
	−1.20	0.857	–	–	10.4	3.95	0.890
	−1.25	0.850	–	–	4.32	2.91	0.904
	−1.30	0.860	–	–	1.86	2.34	0.923
(5)	−1.15	0.671	13.2	0.579	5.32	4.67	0.880
	−1.20	0.686	–	–	9.51	3.70	0.885
	−1.25	0.698	–	–	3.94	2.64	0.906
	−1.30	0.690	–	–	1.68	2.27	0.911

electrodes to compare, but they only inferred that it was very low based on the analysis of the EDS spectra [35,38].

By comparing the values of potential at $j = -100\ mA\ cm^{-2}$ for pure Ni (1) and the best Ni-(Ebonex/Ir) sample (5) (Fig. 7a), it can be concluded that the overvoltage for the HER at sample (5) is for 338 mV lower than that at Ni (1). In comparison with the best Ni-(Ebonex/Ru(10 wt.%)) composite coating [36], the best Ni-(Ebonex/Ir) composite coatings (electrodes 4 and 5) were slightly less active for the HER. The potential at a current density of $-300\ mA\ cm^{-2}$ for the best Ir containing electrode amounts to −1.362 V vs. SCE, while that for the best Ru containing electrode amounts to −1.318 V vs. SCE. The observed difference in activity for the HER between the Ni-(Ebonex/Ir) and Ni-(Ebonex/Ru) composite electrodes can be ascribed to different concentrations of active noble metal sites at the electrode surface. As it was shown, the amount of incorporated Ir was generally lower than the amount of incorporated Ru [36], with the maximum amounts being 1.43 at.% Ir and 2.1 at.% Ru. Besides the reduction in production costs associated with a low amount of used Ir, the main advantage of the Ni-(Ebonex/Ir) composite coatings is the possibility of their application in electrocatalysis of both hydrogen and oxygen evolution, which could greatly facilitate the fabrication of bipolar electrodes for alkaline water electrolyzers. The employment of the same catalyst material on both sides of bipolar electrodes also allows an application of a reverse polarity to a water electrolyzer, which could help to improve the service life of electrodes. The second part of this manuscript will be devoted to the catalytic activity of the Ni-(Ebonex/Ir) composites towards the oxygen evolution reaction.

Conclusions

Codeposition of nickel with suspended Ebonex/Ir(30 wt.%) powder particles produced composite coatings with high electrocatalytic activity for the HER. The employment of

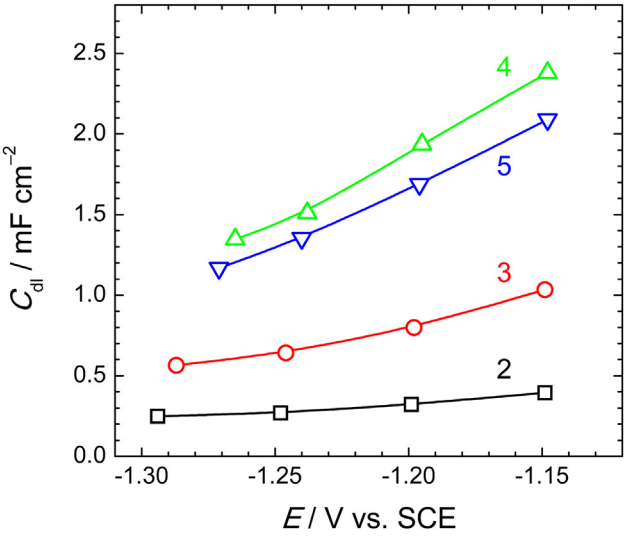

Fig. 10 – The dependence of C_{dl} on potential obtained by analysis of impedance spectra for various Ni-(Ebonex/Ir) samples (marked in the figure).

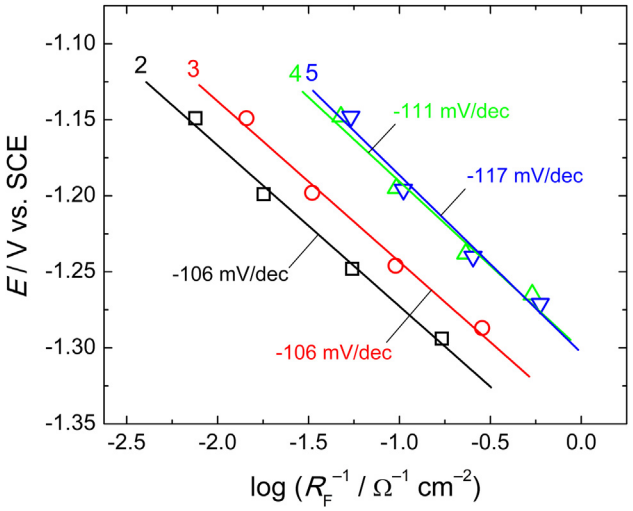

Fig. 11 – The E vs. log R_F dependence obtained by modeling of impedance spectra for various Ni-(Ebonex/Ir) samples (marked in the figure).

Ebonex (Ti_4O_7) particles as a substrate for the Ir nanocatalyst proved to be an efficient method for decreasing the amount of Ir in the final Ni-(Ebonex/Ir) composite electrodes. The most active Ni-(Ebonex/Ir) electrode obtained at 2 g dm^{-3} of Ebonex/Ir particles in a Watts bath (suspension) contained not more than 1.43 at% of Ir. Codeposition of Ni and Ebonex/Ir particles resulted in coatings with increased surface roughness compared to that of a pure Ni deposit prepared under the same experimental conditions. Besides an enhanced electrochemically active surface area, the Ni-(Ebonex/Ir) electrodes also possessed larger intrinsic catalytic activity for the HER than Ni owing to the presence of Ir active sites at the surface.

Acknowledgment

The authors are indebted to the Ministry of Education, Science and Technological Development of the Republic of Serbia for the financial support of this work through the project No. 172054. The authors are grateful to Željko Radovanović of the Innovation Center, Faculty of Technology and Metallurgy, University of Belgrade, for EDS analysis.

REFERENCES

[1] Shervedani RK, Madram AR. Electrocatalytic activities of nanocomposite $Ni_{81}P_{16}C_3$ electrode for hydrogen evolution reaction in alkaline solution by electrochemical impedance spectroscopy. Int J Hydrogen Energy 2008;33:2468–76.
[2] Kubisztal J, Budniok A, Lasia A. Study of the hydrogen evolution reaction on nickel-based composite coatings containing molybdenum powder. Int J Hydrogen Energy 2007;32:1211–8.
[3] Solmaz R, Kardas G. Fabrication and characterization of NiCoZn–M (M: Ag, Pd and Pt) electrocatalysts as cathode materials for electrochemical hydrogen production. Int J Hydrogen Energy 2011;36:12079–87.
[4] Popczyk M, Budniok A, Lasia A. Electrochemical properties of Ni-P electrode materials modified with nickel oxide and metallic cobalt powder. Int J Hydrogen Energy 2005;30:265–71.
[5] Losiewicz B, Budniok A, Rowinski E, Lagiewka E, Lasia A. The structure, morphology and electrochemical impedance study of the hydrogen evolution reaction on the modified nickel electrodes. Int J Hydrogen Energy 2004;29:145–57.
[6] Lasia A. Study of electrode activities towards the hydrogen evolution reaction by a.c. impedance spectroscopy. Int J Hydrogen Energy 1993;18:557–60.
[7] Chen LL, Lasia A. Study of the kinetics of hydrogen evolution reaction on nickel-zinc powder electrodes. J Electrochem Soc 1992;139:3214–9.
[8] Los P, Rami A, Lasia A. Hydrogen evolution reaction on Ni-Al electrodes. J Appl Electrochem 1993;23:135–40.
[9] Herraiz-Cardona I, Ortega E, Pérez-Herranz V. Impedance study of hydrogen evolution on Ni/Zn and NieCo/Zn stainless steel based electrodeposits. Electrochim Acta 2011;56:1308–15.
[10] Endoh E, Otouma H, Marimoto T, Oda Y. New Raney nickel composite-coated electrode for hydrogen evolution. Int J Hydrogen Energy 1987;12:473–9.
[11] Chen LL, Lasia A. Study of the kinetics of hydrogen evolution reaction on Nickel–Zinc alloy electrodes. J Electrochem Soc 1991;138:3321–8.
[12] Okido M, Depo JK, Capuano GA. The mechanism of hydrogen evolution reaction on a modified Raney nickel composite coated electrode by AC impedance. J Electrochem Soc 1993;140:127–33.
[13] Giz MJ, Machado SAS, Avaca LA, Gonzalez ER. High area Ni-Zn and Ni-Co-Zn codeposits as hydrogen electrodes in alkaline-solutions. J Appl Electrochem 1992;22:973–7.
[14] Giz MJ, Bento SC, Gonzalez ER. NiFeZn codeposit as a cathode material for the production of hydrogen by water electrolysis. Int J Hydrogen Energy 2000;25:621–6.
[15] Marozzi CA, Chialvo AC. Development of electrode morphologies of interest in electrocatalysis. Part 1: electrodeposited porous nickel electrodes. Electrochim Acta 2000;45:2111–20.
[16] Marozzi CA, Chialvo AC. Development of electrode morphologies of interest in electrocatalysis: part 2: hydrogen evolution reaction on macroporous nickel electrodes. Electrochim Acta 2001;46:861–6.
[17] Vazquez-Gomez L, Cattarin S, Guerriero P, Musiani M. Preparation and electrochemical characterization of Ni-RuO_2 composite cathodes of large effective area. Electrochim Acta 2007;52:8055–63.
[18] Krstajić NV, Lačnjevac U, Jović BM, Mora S, Jović VD. Non-noble metal composite cathodes for hydrogen evolution. Part II: the Ni-MoO_2 coatings electrodeposited from nickel chloride-ammonium chloride bath containing MoO_2 powder particles. Int J Hydrogen Energy 2011;36:6450–61.
[19] Krstajić NV, Lj Gajić-Krstajić, Lačnjevac U, Jović BM, Mora S, Jović VD. Non-noble metal composite cathodes for hydrogen evolution. Part I: the $NiMoO_x$ coatings electrodeposited from Watt's type bath containing MoO_3 powder particles. Int J Hydrogen Energy 2011;36:6441–9.
[20] Zheng Z, Li N, Wang C-Q, Li D-Y, Zhu Y-M, Wud G. Ni-CeO_2 composite cathode material for hydrogen evolution reaction in alkaline electrolyte. Int J Hydrogen Energy 2012;37:13921–2.
[21] Rosalbino F, Delsante S, Borzone G, Angelini E. Electrocatalytic behaviour of Co-Ni-R (R – Rare earth metal) crystalline alloys as electrode materials for hydrogen evolution reaction in alkaline medium. Int J Hydrogen Energy 2008;33:6696–703.
[22] Vazquez-Gomez L, Cattarin S, Guerriero P, Musiani M. Influence of deposition current density on the composition and properties of electrodeposited Ni + RuO_2 and Ni + IrO_2 composites. J Electroanal Chem 2009;634:42–8.
[23] Iwakura C, Tanaka M, Nakamatsu S, Inoue H, Matsuoka M, Furukawa N. Electrochemical properties of Ni/(Ni + RuO_2) active cathodes for hydrogen evolution in chlor-alkali electrolysis. Electrochim Acta 1995;40:977–82.
[24] Tavares AC, Trasatti S. Ni + RuO_2 co-deposited electrodes for hydrogen evolution. Electrochim Acta 2000;45:4195–202.
[25] Shibli SMA, Dilimon VS. Effect of phosphorous content and TiO_2-reinforcement on Ni-P electroless plates for hydrogen evolution reaction. Int J Hydrogen Energy 2007;32:1694–700.
[26] Lupi C, Dell'Era A, Pasquali M. Nickel-cobalt electrodeposited alloys for hydrogen evolution in alkaline media. Int J Hydrogen Energy 2009;34:2101–6.
[27] Solmaz R, Doner A, Sahin I, Yuce AO, Kardas G, Yazici B, et al. The stability of NiCoZn electrocatalyst for hydrogen evolution activity in alkaline solution during long-term electrolysis. Int J Hydrogen Energy 2009;34:7910–8.
[28] Suffredini HB, Cerne JL, Crnkovic FC, Machado SAS, Avaca LA. Recent developments in electrode materials for water electrolysis. Int J Hydrogen Energy 2000;25:415–23.

[29] Navarro-Flores E, Chong ZW, Omanovic S. Characterization of Ni, NiMo, NiW and NiFe electroactive coatings as electrocatalysts for hydrogen evolution in an acidic medium. J Mol Catal A Chem 2005;226:179–97.
[30] Aaboubi O. Hydrogen evolution activity of NiMo coating electrodeposited under magnetic field control. Int J Hydrogen Energy 2011;36:4702–9.
[31] Rashkov R, Arnaudova M, Avdeev G, Zielonka A, Jannakoudakis P, Jannakoudakis A, et al. NiW/TiOx composite layers as cathode material for hydrogen evolution reaction. Int J Hydrogen Energy 2009;34:2095–100.
[32] Solmaz R, Kardas G. Electrochemical deposition and characterization of NiFe coatings as electrocatalytic materials for alkaline water electrolysis. Electrochim Acta 2009;54:3726–34.
[33] Han Q, Chen J, Liu K, Li X, Wei X. The heat-treatment effect of amorphous Ni-S(La) term electrode on the hydrogen evolution reaction in an alkaline media. Int J Hydrogen Energy 2004;29:597–603.
[34] Bianchi I, Guerrini E, Trasatti S. Electrocatalytic activation of Ni for H_2 evolution by spontaneous deposition of Ru. Chem Phys 2005;319:192–9.
[35] Vazquez-Gomez L, Cattarin S, Guerriero P, Musiani M. Hydrogen evolution on porous Ni cathodes modified by spontaneous deposition of Ru or Ir. Electrochim Acta 2008;53:8310–8.
[36] UČ Lačnjevac, Jović BM, Jović VD, Radmilović VR, Krstajić NV. Kinetics of the hydrogen evolution reaction on Ni-(Ebonex-supported Ru) composite coatings in alkaline solution. Int J Hydrogen Energy 2013;38:10178–90.
[37] Kuttiyiel KA, Sasaki K, Chen W, Sub D, Adzic RR. Core–shell, hollow-structured iridium–nickel nitride nanoparticles for the hydrogen evolution reaction. J Mater Chem A 2014;2:591–4.
[38] Vazquez-Gomez L, Cattarin S, Gerbasi R, Guerriero P, Musiani M. Activation of porous Ni cathodes towards hydrogen evolution by electrodeposition of Ir nuclei. J Appl Electrochem 2009;39:2165–72.
[39] Lamy-Pitara E, Barbier J. The electrocatalytic reactions of oxidation and evolution of hydrogen on iridium electrodes modified by sulphur adsorption. J Electroanal Chem 1996;416:47–51.
[40] Boodts JCF, Trasatti S. Hydrogen evolution at iridium oxide cathodes. J Appl Electrochem 1989;19:255–62.
[41] Solmaz R. Electrochemical preparation and characterization of C/Ni–NiIr composite electrodes as novel cathode materials for alkaline water electrolysis. Int J Hydrogen Energy 2013;38:2251–6.
[42] He L, Huang Y, Liu XY, Li L, Wang A, Wang X, et al. Structural and catalytic properties of supported Ni–Ir alloy catalysts for H_2 generation via hydrous hydrazine decomposition. Appl Catal B Environ 2014;147:779–88.
[43] Gileadi E. Electrode kinetics for chemists, chemical engineers, and materials scientists. New York: VCH Publishers, Inc.; 1993.
[44] Sattar MA, Conway BE. Electrochemistry of the nickel oxide electrode VI. Surface oxidation of nickel anodes in alkaline solution. Electrochim Acta 1969;14:695–710.
[45] Bode H, Dehmelt K, Witte J. Zur kenntnis der nickelhydroxidelektrode—I.Über das nickel (II)-hydroxidhydrat. Electrochim Acta 1966;11:1079–87.
[46] Babić B, Kaluđerović B, Lj Vračar, Krstajić N. Characterization of carbon cryogel synthesized by sol-gel polycondensation and freeze-drying. Carbon 2004;42:2617–24.
[47] Bockris JOM, Otagava T. The electrocatalysis of oxygen evolution on perovskites. J Elerctrochem Soc 1984;131:290–302.
[48] Armstrong RD, Henderson M. Impedance plane display of a reaction with an adsorbed intermediate. J Electroanal Chem 1972;39:81–90.
[49] Harrington DA, Conway BE. AC impedance of faradaic reactions involving electrosorbed intermediates–I. Kinetic theory. Electrochim Acta 1987;32:1703–12.
[50] Brug GJ, Van den Eeden ALG, Sluyters-Rehbach M, Sluyters JH. The analysis of electrode impedances complicated by the presence of a constant phase element. J Electroanal Chem 1984;176:275–95.
[51] Jović BM, UČ Lačnjevac, Krstajić NV, Jović VD. Service life test of the NiSn coatings as cathodes for hydrogen evolution in industrial chlor-alkali electrolysis. Int J Hydrogen Energy 2014;39:8947–58.